JOURNAL OF MATERIALS SCIENCE 12 (1977) 1598–1604

Creep mapping in a polycrystalline ceramic: application to magnesium oxide and magnesiowustite

J. D. HODGE*, P. A. LESSING†, R. S. GORDON
Department of Materials Science and Engineering, University of Utah, Salt Lake City, Utah, USA

The construction of deformation mechanism maps for a polycrystalline ionic solid in which anion and cation transport are coupled has been demonstrated. Because of anion–cation ambipolar coupling, two regimes of Coble creep are possible in systems where anion grain boundary transport is rapid: (1) rate-controlled at low temperatures and small grain sizes by cation grain-boundary diffusion, and (2) rate-limited at high temperatures and large grain sizes by anion grain-boundary diffusion. A new type of deformation mechanism map was introduced in which the temperature and grain size were primary variables. This map was shown to be particularly useful for materials which deform primarily by diffusional creep mechanisms. Ambipolar diffusional creep theory was used to construct several deformation mechanism maps for polycrystalline MgO and magnesiowustite over wide ranges of stress, grain size, temperature and composition.

1. Introduction

Creep diagrams (or deformation mechanism maps) have recently come into widespread use as a simple graphical method for presenting a wealth of information on a polycrystalline material's mechanical properties over a range of engineering variables [1]. Weertman [2, 3] first suggested the use of creep diagrams in which stress was plotted as a function of temperature at a constant grain size. To aid in comparison between various material types, the plotted stress was normalized with respect to the material's shear modulus and the temperature was normalized with respect to the melting temperature. Mohamed and Langdon [4, 5] later suggested a second type of map in which the grain size, normalized with respect to the material's Burger's vector, is plotted against a normalized stress at a constant temperature. Both of these maps have proven extremely useful, especially for materials which can deform by a variety of different mechanisms. However, maps published in the past for ceramic materials have generally been constructed using large extrapolations of limited experimental creep or mass transport data with the result that these maps can be inaccurate over large ranges of stress, temperature, and grain size. Furthermore, these maps have been based, in part, on diffusional creep theories which are only appropriate for metallic systems in which a single diffusing species governs mass transport.

Our objective in this paper will be (1) to outline the construction of creep maps for a polycrystalline ceramic solid in which ambipolar (coupled ionic) diffusion is important, (2) to introduce a new type of deformation map, which is especially useful for materials which deform extensively by diffusional mechanisms, whereby temperature and grain size are the primary variables under conditions of constant stress, and (3) to illustrate the foregoing by presenting maps of deformation in polycrystalline MgO and magnesiowustite which

*Present address: Massachusetts Institute of Technology, Cambridge Massachusetts, USA.
†Present address: Los Alamos Scientific Laboratory, Los Alamos, New Mexico, USA.

have been constructed using creep data taken over wide ranges of stress, temperature, grain size, and composition.

2. Construction of deformation maps

The data, which were used for the construction of deformation maps, were taken from several sources [6–9]. Diffusional creep in these materials is characterized by a strong inverse relationship between the strain-rate ($\dot{\epsilon}$) and grain size (GS) and by creep rates which increase with the concentration of trivalent iron in solid solution [6, 7]. At higher stresses and larger grain sizes, viscous deformation gives way to power law or non-viscous deformation which can be described by the following relations [8, 9]:

pure MgO*

$$\dot{\epsilon}(\mathrm{h}^{-1}) = 1300\,\sigma^{3.0}\exp\left(\frac{-80\,000\ \mathrm{cal\,mol}^{-1}}{RT}\right) \quad (1a)$$

Fe-doped MgO*

$$\dot{\epsilon}(\mathrm{h}^{-1}) = 31.2\,\sigma^{3.0}\exp\left(\frac{-71\,000\ \mathrm{cal\,mol}^{-1}}{RT}\right). \quad (1b)$$

In contrast to the diffusional creep regimes, non-viscous creep in pure and iron-doped polycrystalline MgO is characterized by a higher stress (σ) exponent (≈ 3) and creep rates which are independent of grain size and nearly independent of the iron dopant concentration.

In diffusional creep regimes, some lattice diffusion coefficients were calculated from the creep data using the Nabarro–Herring equation, i.e.†

$$\dot{\epsilon} = \frac{14\,\Omega_v \sigma D^l_{Mg}}{kT(GS)^2} \quad (2)$$

For those deformation regimes which were intermediate between Nabarro–Herring and Coble creep [6], the following equations derived by Gordon [10, 11] were applied to the creep data using previously reported procedures [11, 12] to determine values of the lattice (D^l) and grain-boundary diffusion (δD^b) coefficients.‡

$$\dot{\epsilon} = \frac{44\,\Omega_v \sigma}{\Pi kT(GS)^2}\left[\frac{D^l_{Mg}}{1 + \dfrac{GS}{\Pi}\dfrac{D^l_{Mg}}{\delta_0 D^b_0}}\right] \quad (3)$$

$$\dot{\epsilon} = \frac{44\,\Omega_v \sigma}{kT(GS)^3}\left[\left(\frac{GS}{\Pi}\right)D^l_{Mg} + \delta_{Mg}D^b_{Mg}\right]. \quad (4)$$

Equation 3 refers to regimes in which both magnesium lattice and oxygen grain-boundary diffusion contribute significantly to the creep rate, and Equation 4 refers to regimes where both magnesium lattice and grain-boundary diffusion are comparable. In the experimental range appropriate for these materials, no evidence was found for creep controlled solely by grain-boundary diffusion either cation or anion.

In those maps where they were required, the activation energy for magnesium lattice diffusion was taken from experimental creep data [6]. The activation energy for oxygen grain-boundary diffusion was estimated from experimental creep data by Hodge [13] and the activation energy (upper limit) for magnesium grain-boundary diffusion was estimated from tracer diffusion studies [14]. A summary of the data used in these maps is presented in Tables I and II.

Deformation mechanism maps were constructed using Equations 1 to 4 and the data in Tables I and II to plot a number of iso-strain-rate lines for each mechanism. Boundaries between mechanisms were then inserted by using the locus of points at the intersection of two sets of iso-strain-rate lines. In assigning these boundaries and fields, a mechanism was assumed to be controlling when it resulted in the highest possible strain-rate at the lowest possible set of variables (temperature, grain size, or stress). This assumption was good for all boundaries except those separating regimes controlled by magnesium lattice and oxygen grain-boundary diffusion. For this case, because of the coupled nature of the diffusion between the cation and anion, the foregoing statement must be reversed in that the mechanism giving the lowest possible strain rate at the highest possible set of variables will be rate controlling. Because of the complex nature of the equations involved, the iso-strain-rate lines on the temperature versus grain size maps were computer generated.

It should be noted that boundary lines represent situations where the creep rates of the two processes in question are equal. It must be remembered that in the vicinity of the boundaries defor-

*The units of stress (σ) are MN m^{-2}.

†Ω_v is the MgO molecular volume (1.86×10^{-23} cm^3), k is Boltzmann's constant, and T is the absolute temperature.

‡δD^b is actually the product of the grain-boundary width (δ) and the grain-boundary diffusivity (D^b).

TABLE I Diffusion coefficients at 1350° C for the MgO–FeO–Fe_2O_3 system

Dopant (cation % Fe)	D^l_{Mg} ($cm^2 sec^{-1}$)	$\delta_{Mg}D^b_{Mg}$ ($cm^3 sec^{-1}$)	$\delta_0 D^b_0$ ($cm^3 sec^{-1}$)	Reference
2.65	9.0×10^{-12}	–	1.6×10^{-14}	[6]
0.53	2.3×10^{-12}	–	–	[6]
0.05	4.8×10^{-13}	7.3×10^{-16}	–	[7]
Undoped	3.6×10^{-13}	$>10^{-17}$	–	[7]
Mg tracer*	1.15×10^{-12}	–	–	[14]

* Included for comparison.

TABLE II Activation energies for diffusion in the MgO–FeO–Fe_2O_3 system

Mechanism	Activation energy (kcal mol^{-1})	Reference
Magnesium lattice	117	[6]
Magnesium grain boundary	$\leqslant 64$	[14]
Oxygen grain boundary	~ 35*	[13]

* Obtained from an analysis of the activation energy for a diffusional creep regime in which magnesium lattice and oxygen grain-boundary diffusion are comparable [13].

mation modes are mixed. In particular mixed modes of deformation may exist in diffusional creep regimes over several orders of magnitude in strain-rate.*

3. Deformation maps at constant temperature

Deformation mechanism maps for polycrystalline MgO and magnesiowustite in an air atmosphere are shown in Figs. 1 to 3. In these maps the stress has been plotted against grain size at a constant temperature (1350° C) in a manner similar to the procedure introduced by Langdon [4, 5]. Referring to Fig. 1 it can be seen that only two deformation mechanisms operate in undoped, polycrystalline MgO: a non-viscous mechanism which dominates at large grain sizes and high stresses and a diffusional creep mechanism controlled by magnesium lattice diffusion (Nabarro–Herring creep) which is dominant at low stresses and small grain sizes. It is noted that as the grain size increases, the transition from diffusion con-

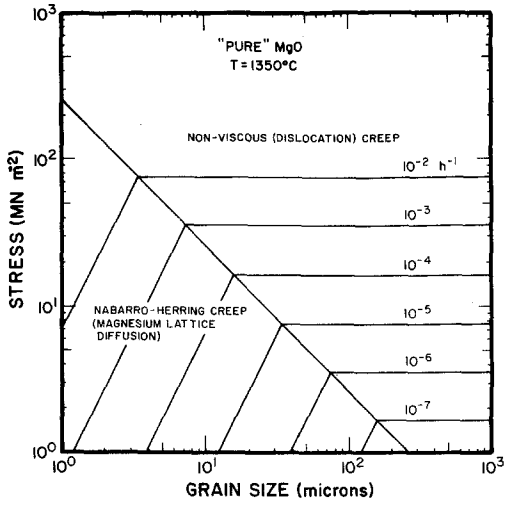

Figure 1 Deformation mechanism map for undoped polycrystalline MgO at 1350° C.

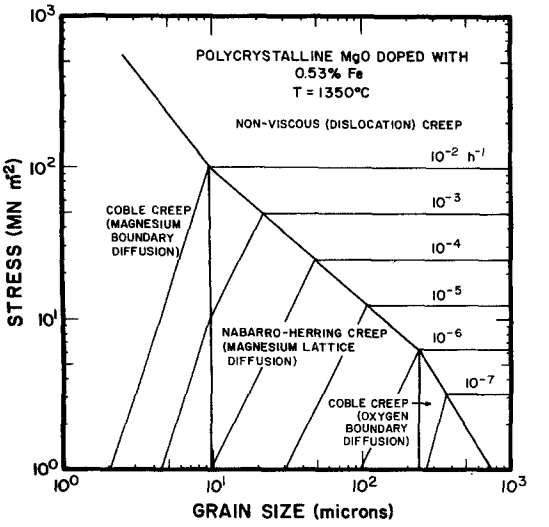

Figure 2 Deformation mechanism map at 1350° C for polycrystalline MgO doped with 0.53 cation % iron.

*Unlike previous deformation maps, maps constructed for this paper were not normalized. This procedure while making comparison with other materials more difficult, presents creep data in an easier-to-understand form and allows for direct comparison with experimental creep data.

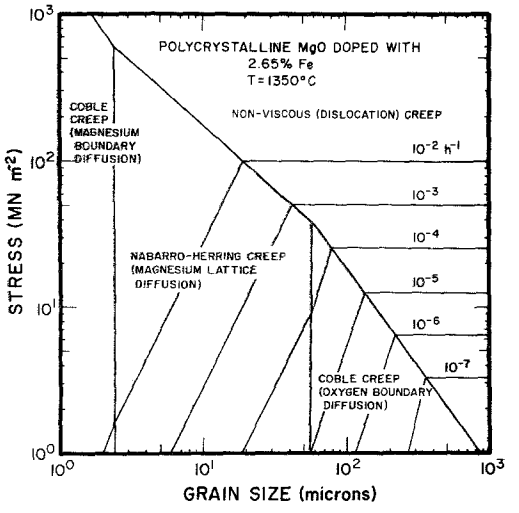

Figure 3 Deformation mechanism map at 1350° C for polycrystalline MgO doped with 2.65 cation % iron.

trolled creep to non-viscous creep occurs at lower stresses. Magnesium lattice diffusion is assumed to be rate-controlling [10, 11]. Previous deformation reported [15] to be a fast diffusion path for oxygen. In addition, the magnesium lattice diffusion coefficient inferred from creep data (Table I) is in reasonable agreement with the cation tracer value. Because of rapid oxygen grain-boundary diffusion, ambipolar diffusional creep theory predicts that at low lattice diffusivities (i.e. low impurity levels) magnesium lattice diffusion will be rate-controlling [10, 11]. Previous deformation maps [5] have been constructed assuming that oxygen lattice and/or grain-boundary diffusion are rate controlling in polycrystalline MgO. However, ambipolar diffusional creep [10, 11] theory demonstrates that oxygen grain-boundary diffusion will be rate controlling only at very large grain sizes ($>200\,\mu$m) and at very small stresses and that oxygen lattice diffusion will never be rate-controlling in an extrinsic ionic compound in which rapid anion grain-boundary diffusion takes place. Creep maps which are constructed from constitutive equations based on a single diffusing species (i.e. metals) will give erroneous conclusions when applied to the diffusional creep of a polycrystalline ionic compound in which anion and cation diffusion are coupled and in which mass transport can take place in parallel over more than one path.

The effect of doping polycrystalline MgO with 0.53 cation % Fe is shown in Fig. 2 in a second constant temperature deformation map. Because doping with trivalent iron enhances diffusion (especially cation lattice diffusion), there is an expansion of the diffusional creep fields in the doped system over that which existed in undoped MgO. Consequently, the transition from diffusion controlled creep to non-viscous creep occurs at higher stresses and larger grain sizes since the non-viscous creep rates are essentially independent of the iron dopant concentration [8, 9].

Three diffusional creep mechanisms are indicated in the viscous regime: (1) Coble creep controlled by magnesium grain-boundary diffusion at grain sizes below about $10\,\mu$m, (2) Nabarro–Herring creep controlled by magnesium lattice diffusion for intermediate grain sizes (10 to $250\,\mu$m), and (3) Coble creep controlled by oxygen grain-boundary diffusion at very large sizes ($>250\,\mu$m). All of the experimental data to date have fallen in the intermediate grain size range which is controlled by Nabarro–Herring creep. Experiments at smaller grain sizes are complicated by problems associated with specimen fabrication and excessive grain growth. At larger grain sizes creep rates become undetectable ($\leqslant 10^{-6}\,h^{-1}$) at the stress levels required for diffusional creep ($<5.0\,MN\,m^{-2}$). Because of this, diffusion coefficients for magnesium and oxygen grain-boundary diffusion were estimated from those values obtained at the 0.05 cation % and the 2.65 cation % dopant levels, respectively.

In Fig. 3 a third constant temperature map is shown for a higher (2.65 cation % iron) dopant level. Here, as was shown in the previous map, the diffusional creep fields have expanded significantly over what they were at the lower dopant level due to the enhancement of diffusional processes by the presence of trivalent iron. Because the presence of trivalent iron causes a significant enhancement in the magnesium lattice diffusivity compared to relatively smaller effects on magnesium and oxygen grain-boundary diffusion, the extent of the diffusional creep regime controlled by magnesium boundary diffusion has decreased from what it was at the lower dopant concentration and the regime controlled by oxygen boundary diffusion has increased. It is interesting to note that any increase in the magnitude of the magnesium lattice diffusivity due to a change in the defect structure will cause a decrease in the regime controlled by magnesium grain-boundary diffusion and to a comparable increase in the regime which is rate limited by oxygen

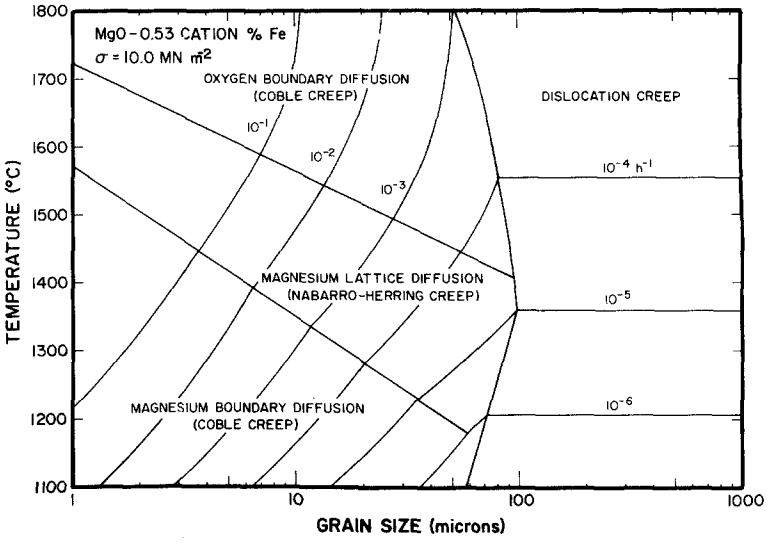

Figure 4 Deformation mechanism map at constant stress for polycrystalline MgO doped with 0.53 cation % iron.

grain-boundary diffusion. These effects are in accord with that predicted by the ambipolar diffusional creep theory [10, 11].

The creep data obtained at this dopant level extended into both the regimes controlled by magnesium lattice and oxygen grain-boundary diffusion. However, for reasons given earlier, experiments at grain sizes below about 10 μm proved difficult and therefore the value of the magnesium boundary diffusion was estimated from the value obtained in experiments* at an iron concentration of 0.05 cation %.

4. Deformation maps as constant stress

In Figs. 4 and 5, deformation mechanism maps for polycrystalline MgO doped with 0.53 and 2.65 cation % Fe, respectively, are shown wherein the grain size has been plotted against temperature at a constant stress (10.0 MN m^{-2}) for creep tests in air.† This new type of map is particularly useful for materials which deform primarily via diffusional mechanisms because the creep rate is much more sensitive to changes in temperature and grain size than it is to changes in stress.

Several interesting features are readily apparent in these maps. Two regimes of Coble creep (i.e. $\dot{\epsilon} \propto GS^{-3}$) are present, one at low temperatures and small grain sizes (magnesium grain-boundary diffusion) and the other at high temperatures and large grain sizes (oxygen grain-boundary diffusion). This type of behaviour is strikingly different from that observed in metals (single diffusing species) for which Coble creep is predicted only at low temperatures and for small grain sizes. Since the activation energy for grain-boundary diffusion is likely less than that for lattice diffusion, the transition grain sizes between adjacent Coble and Nabarro–Herring regimes decrease as the temperature is increased. The transition to non-viscous creep (Figs. 4 and 5) is curved because of the mixed nature of creep in the diffusional regime which results in an activation energy for creep which is temperature dependent. It approaches ~64 kcal mol^{-1} at low temperatures where magnesium grain-boundary diffusion is controlling, 117 kcal mol^{-1} at intermediate temperatures where magnesium lattice diffusion is important, and ~35 kcal mol^{-1} at high temperatures where oxygen grain-boundary diffusion is dominant. Consequently, the non-viscous transition occurs at a maximum grain size in the region where magnesium lattice diffusion is dominant and decreases with either increasing or decreasing temperature as either magnesium or oxygen grain-boundary diffusion becomes rate-limiting. Also, as was the case in the constant temperature maps, as the stress is increased the non-viscous modes will become dominant at smaller grain sizes in these constant stress deformation maps.

*In these experiments the grain size dependence and the relevant mass transport parameters were deduced from the correlation between transient creep and simultaneous grain growth [7, 16].

†Since the stress is constant, these maps may be regarded as a horizontal section cut through a map at constant temperature.

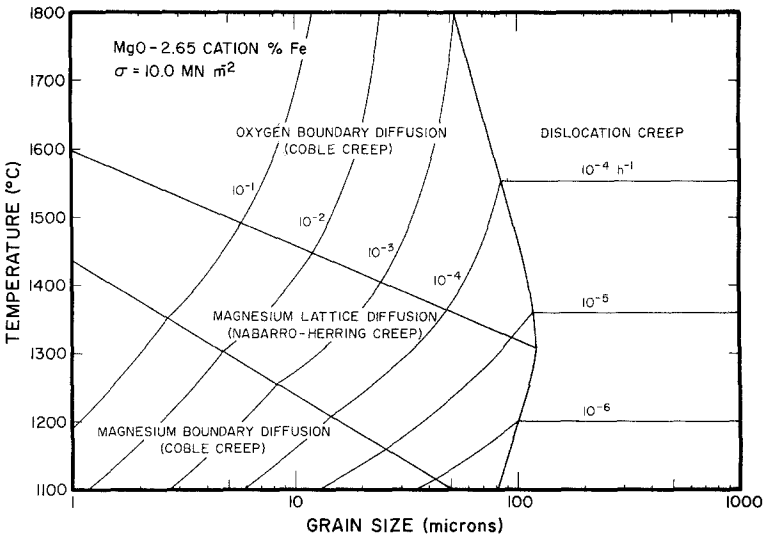

Figure 5 Deformation mechanism map at constant stress for polycrystalline MgO doped with 2.65 cation % iron.

It is noted, that due to the enhancing effect of trivalent iron on magnesium lattice diffusion, the transitions between adjacent Coble and Nabarro–Herring creep regimes occur at higher temperatures and larger grain sizes as the dopant level is decreased. This behaviour is consistent with that shown in the constant temperature maps wherein an increase in the magnesium lattice diffusivity caused a decrease in the magnesium boundary diffusion controlled field and a corresponding increase in the regime controlled by the oxygen boundary diffusion.

At the 0.53% dopant concentration, most of the experimental data taken in the diffusional regime fell in the Nabarro–Herring field. For this reason, diffusivities used for magnesium and oxygen grain-boundary diffusion were estimated from creep experiments at the 0.05 cation % and 2.65 cation % dopant concentrations, respectively. With respect to the experimental range at the 2.65% dopant level much of the deformation in the diffusion controlled regime is mixed in character, i.e. $[(GS)/\Pi]D^{l}_{Mg} \approx \delta_0 D^{b}_{0}$. Consequently, both the magnesium lattice and the oxygen grain-boundary diffusion coefficients were calculated using the analysis developed by Gordon and Hodge [12]. The magnesium grain-boundary diffusion coefficient was estimated from the value obtained experimentally at the 0.05 cation % Fe dopant level. Finally, the non-viscous regime at the 2.65% dopant concentration was assumed to be identical to that measured experimentally at the 0.53% dopant level at large grain sizes ($<100\,\mu m$) [8].

5. Conclusion

The construction of deformation mechanism maps for a polycrystalline ionic solid in which anion and cation transport are coupled has been demonstrated. Because of anion–cation ambipolar coupling, two regimes of Coble creep are possible in systems where anion grain-boundary transport is rapid: (1) at low temperatures and small grain sizes rate-controlled by cation grain-boundary diffusion and (2) at high temperatures and large grain sizes rate-controlled by anion grain-boundary diffusion.

A new type of deformation mechanism map was introduced in which the temperature and grain size were primary variables. This map was shown to be particularly useful for materials which deform primarily by diffusional mechanisms.

Ambipolar diffusional creep theory was used to construct several deformation mechanism maps in the MgO and MgO–FeO–Fe_2O_3 systems over a wide range of experimental variables which included stress, grain size, temperature and composition.

Acknowledgement

This research was supported by the Energy Research and Development Administration under Contract E(11-1)-1591.

References

1. M. F. ASHBY, *Acta Met.* **20** (1972) 887.
2. J. WEERTMAN and J. R. WEERTMAN, "Physical Metallurgy", edited by R. W. Cahn (North-Holland, Amsterdam, 1965) p. 793.

3. J. WEERTMAN, *Trans. Amer. Soc. Metals* **61** (1968) 681.
4. F. A. MOHAMED and T. G. LANGDON, *Met. Trans.* **5** (1974) 2339.
5. T. G. LANGDON and F. A. MOHAMED, *J. Mater. Sci.* **11** (1976) 317.
6. R. T. TREMPER, R. A. GIDDINGS, J. D. HODGE and R. S. GORDON, *J. Amer. Ceram. Soc.* **57** (1974) 421.
7. R. S. GORDON, P. A. LESSING and J. D. HODGE, unpublished work.
8. P. A. LESSING and R. S. GORDON, "Deformation in Ceramic Materials", edited by R. C. Bradt and R. E. Tressler (Plenum Press, New York, 1975) p. 271.
9. P. A. LESSING, Ph.D. Thesis, University of Utah (1976).
10. R. S. GORDON, *J. Amer. Ceram. Soc.* **56** (1973) 147.
11. *Idem,* "Mass Transport Phenomena in Ceramics", edited by A. R. Cooper and A. H. Heuer (Plenum, New York, 1975) p. 445.
12. R. S. GORDON and J. D. HODGE, *J. Mater. Sci.* **10** (1975) 200.
13. J. D. HODGE, P. A. LESSING and R. S. GORDON, unpublished work.
14. B. J. WUENSCH, W. C. STEELE and T. VASILOS, *J. Chem. Phys.* **58** (1973) 5258.
15. B. H. HASHIMOTO, M. HAMA and S. SHIRASAKI, *J. Appl. Phys.* **43** (1972) 4828.
16. G. R. TERWILLIGER, H. K. BOWEN and R. S. GORDON, *J. Amer. Ceram. Soc.* **53** (1970) 241.

Received 29 October and accepted 22 November 1976.